3G5 Lab Report

Tahmid Azam

October 2025

Abstract

This study investigates the properties of agarose hydrogels at 3% w/v in plain and 1% $NaNO_3$ formulations. Thermal and optical methods were used to determine the gelling point, with thermal measurements indicating a transition at 55 °C to 57 °C and optical measurements at 36 °C to 37 °C. The addition of salt had only a marginal effect, with differences between plain and salted agarose falling within the experimental margin of error, while discrepancies between the two methods were attributed to methodological differences. Mechanical behaviour under compressive loads (385 g and 925 g) was characterised via creep compliance and fitted using a four-component Burgers model and non-linear least squares regression, demonstrating non-linear viscoelasticity. Swelling studies showed minimal water uptake in agarose, contrasted with significant gelatin swelling. Salt increased compliance and likely expanded pore size through ionic interactions. Overall, these results highlight how ionic content and mechanical stress influence the coil-to-helix transition, viscoelastic response, and swelling of agarose independent of salt content, providing insights for hydrogel design in biomedical applications while confirming the material's softness and suitability for such uses.

1 Introduction

Hydrogels are 3-dimensional polymer networks that are hydrophilic, confering an ability to retain large volumes of water all while maintaing a defined structure [1]. Their high water content is suited to biomedical applications, such as cell culture scaffolds, controlled drug release systems [2], wound dressings, and tissue engineering. Agarose is a naturally occurring polysaccharide polymer, derived from red algae. The polymer structure is linear, composed of D-galactose and 3,6-anhydrous-L-galactose monomers forming molecules of molecular weight between 80 kDa and 140 kDa. Their structure involves curly coils, double helices, and an aggregated double helix network, structures that form sensitive to heating or cooling. Agarose hydrogels are thermoreversible, show good biocompatability, are relatively inert, and have tunable mechanical properties [3].

In this study, we investigate agarose hydrogels formed at 3% w/v, in a plain formulation and a salted formulation with added $NaNO_3$ at 1% w/v. We investigate material properties of the hydrogels: the gelling point using thermal (S1) and optical (S2) methods; the mechanical response under compression (S3); and the swelling behaviour in water (S4). The effect of added salt on these properties is considered. These investigations can be used to inform the design of agarose hydrogels for biomedical applications.

2 Investigations

2.1 Thermal measurement of gelling point (S1)

2.1.1 Introduction

The gelling point is a material property that describes the temperature at which agarose transitions from a liquid to a solid. In this experiment, the temperature of heated samples of plain and salted agarose was monitored during cooling in a chilled water bath for 30 min at a sampling frequency of 1 Hz using a thermocouple.

Newton's Law of Cooling (stated in Figure 1) motivates defining the gelling point as the temperature at which the linear relationship between $\ln \Delta T$ and time no longer holds.

$$\frac{dT}{dt} \propto T - T_a$$

Figure 1: Newton's Law of cooling dictates that the rate of change of a hot body's temperature via convective heat loss is proportional to the difference of its temperature T and the ambient temperature T_a.

During the phase transition, agarose undergoes a coil-to-helix conformational change, during which thermal energy is absorbed, causing the rate of temperature decrease to exceed that stated by Newton. The ambient temperature, T_a, is taken as the final temperature recorded at 1800 s. In this experiment we assume the factors affecting the constant of proportionality in Newton's Law of Cooling (e.g., body's geometry, the fluid the body is immersed in) remain constant, which allows us to attribute the deviation from linearity to changes in the body's internal energy and the associated phase change-associated enthalpy.

2.1.2 Results

The cooling curves for plain and salted agarose gels, plotted as $\ln \Delta T$ against time t, are shown in Figure 2 and Figure 3, respectively. A linear region of the curve, selected by inspection for $60 \leq t \leq 150$ s, is used to fit a linear regression representing the Newton cooling rate. The resulting regression equation is shown on the top-right of each $\ln \Delta T$ plot and is extrapolated over the full time range (0–1800 s). Residuals, defined as the difference between the observed $\ln \Delta T$ values and the regression fit, are plotted on the lower axes. The gelling point is identified as the first time at which the residuals exceed three standard deviations of the residuals in the linear region. The gelling points determined for plain and salted agarose gels using this method are summarised in Table 1. We find the gelling point for salted agarose to by 2.1 °C higher than plain agarose.

	S1 T_g (°C)	S2 T_g (°C)
Plain agarose	54.7	37.0
Salted agarose	56.8	36.2

Table 1: Gelling points for plain and salted agarose gels

2.1.3 Limitations

Limitations of the method may have introduced uncertainty into our observed gelling points. The thermocouples were not perfectly calibrated, uncertainty observed during the practical as multiple thermocouples in the same water bath were reading values up to 1 °C apart. Local temperature gradients may have arised from multiple experiments being run in parallel with hot agarose gels being introduced to the water bath and removed, resulting in an inconsistent level of cooling. Furthermore, the water bath was not stirred, nor was the agarose solution inside the vessel, and the thermocouple was not perfectly placed in the centre of the vessel in all cases. The ambient temperature was taken as the last recorded temperature at the end of the experiment, which may not reflect the actual temperature of the water bath if equilibrium was not achieved.

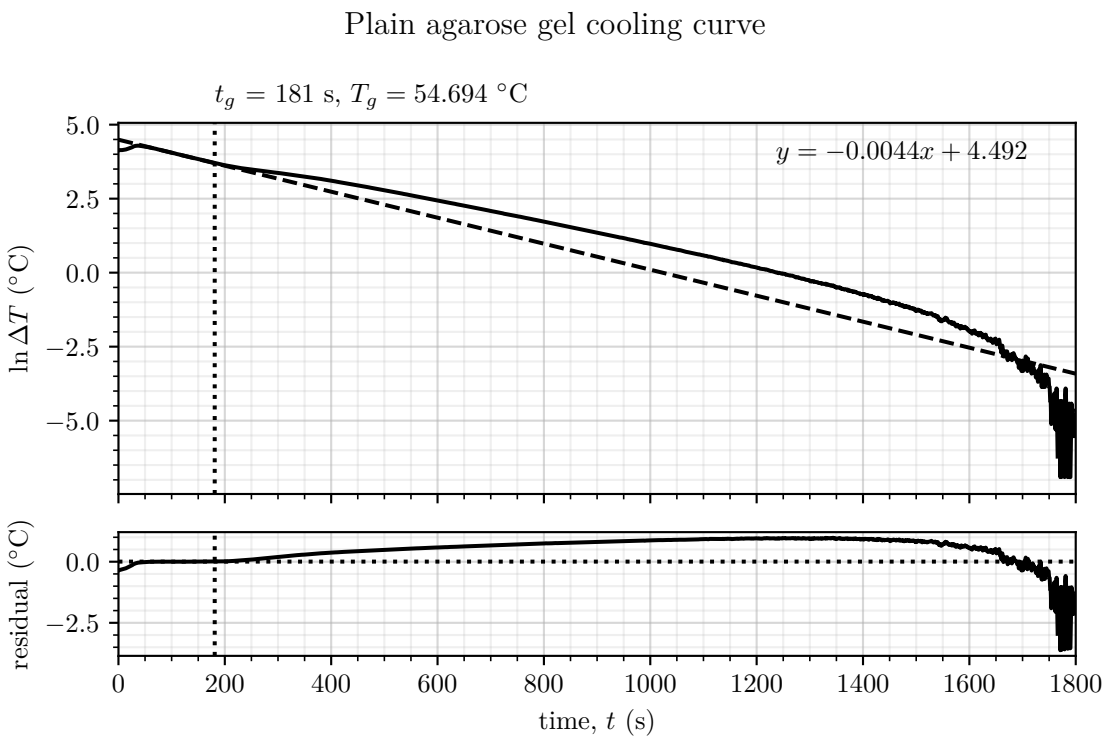

Figure 2: Plain agarose gel cooling curve

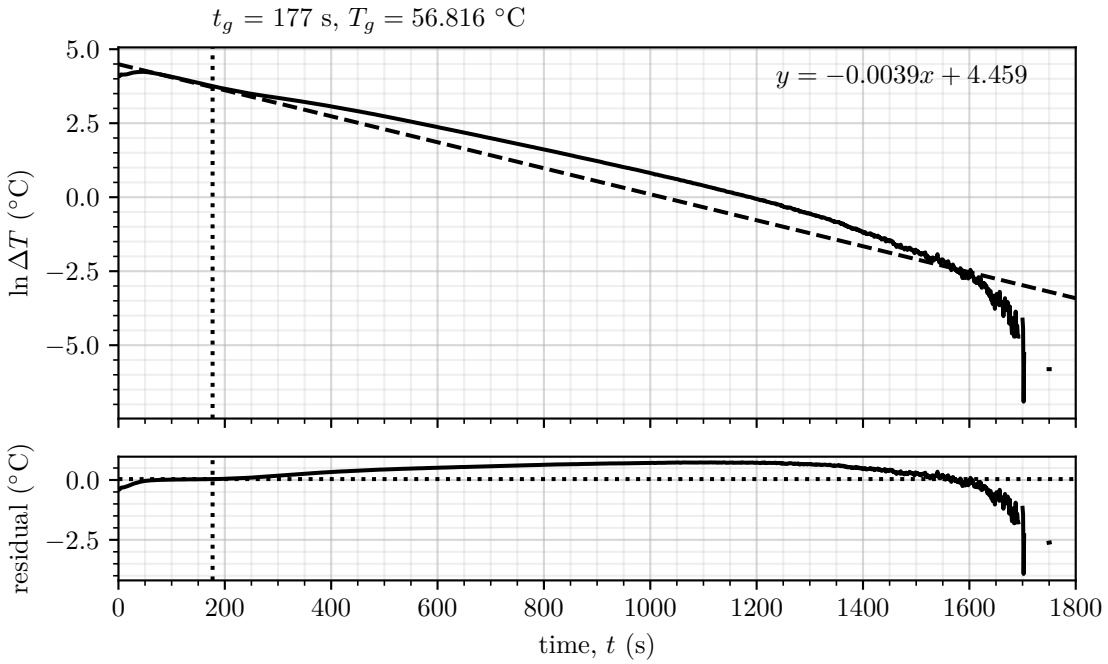

Figure 3: Salted agarose gel cooling curve

2.2 Optical measurement of gelling point (S2)

2.2.1 Introduction

During the coil-to-helix transition the interaction of agarose with light changes in addition to enthalpy outlined exploited in the thermal measurement experimental method. The solution is observed to transition from transparent to cloudy, which can be measured using a scanning spectrophotometer, which passes a light (in this case, wavelength, $\lambda = 400\,\text{nm}$) through the sample and measures how much is absorbed. The temperature is also monitored using a thermocouple. Both the absorbance and temperature are sampled at 0.1 Hz.

2.2.2 Results

The temperature and absorbance curves for plain and salted agarose gel are plotted in Figure 4 and Figure 5 respectively. A mask of $60 \geq t \geq 800$ is determined to constitue a baseline by inspection, and baseline is determined by finding the average (equivalent to regression with a model of $y = c$, where c is a constant). The baseline is extrapolated for all t. The residuals, defined as the difference between the absorbance values and the fitted baseline, are plotted in the bottom axes. The gelling point is identified as the first time at which the residuals exceed three standard deviations of the residuals in the masked region. The gelling points determined for plain and salted agarose gels using this method are summarised in Table 1. The gelling point of salted agarose is found to be 0.8 °C lower than plain agarose.

2.2.3 Limitations

The limitations of the thermocouple outlined in 2.1.3 also apply to this method (thermocouple uncertainty, placement, mixing). In addition, the spectrophotometer may not have been perfectly calibrated, and we assume that the mechanism in the spectrophotometer can effectively isolate the sample from any ambient light. We also assume that the cuvette, the vessel that held the agarose solution, was optically transparent; and that 400 nm is an effective wavelength to capture the change in absorbance during gelation.

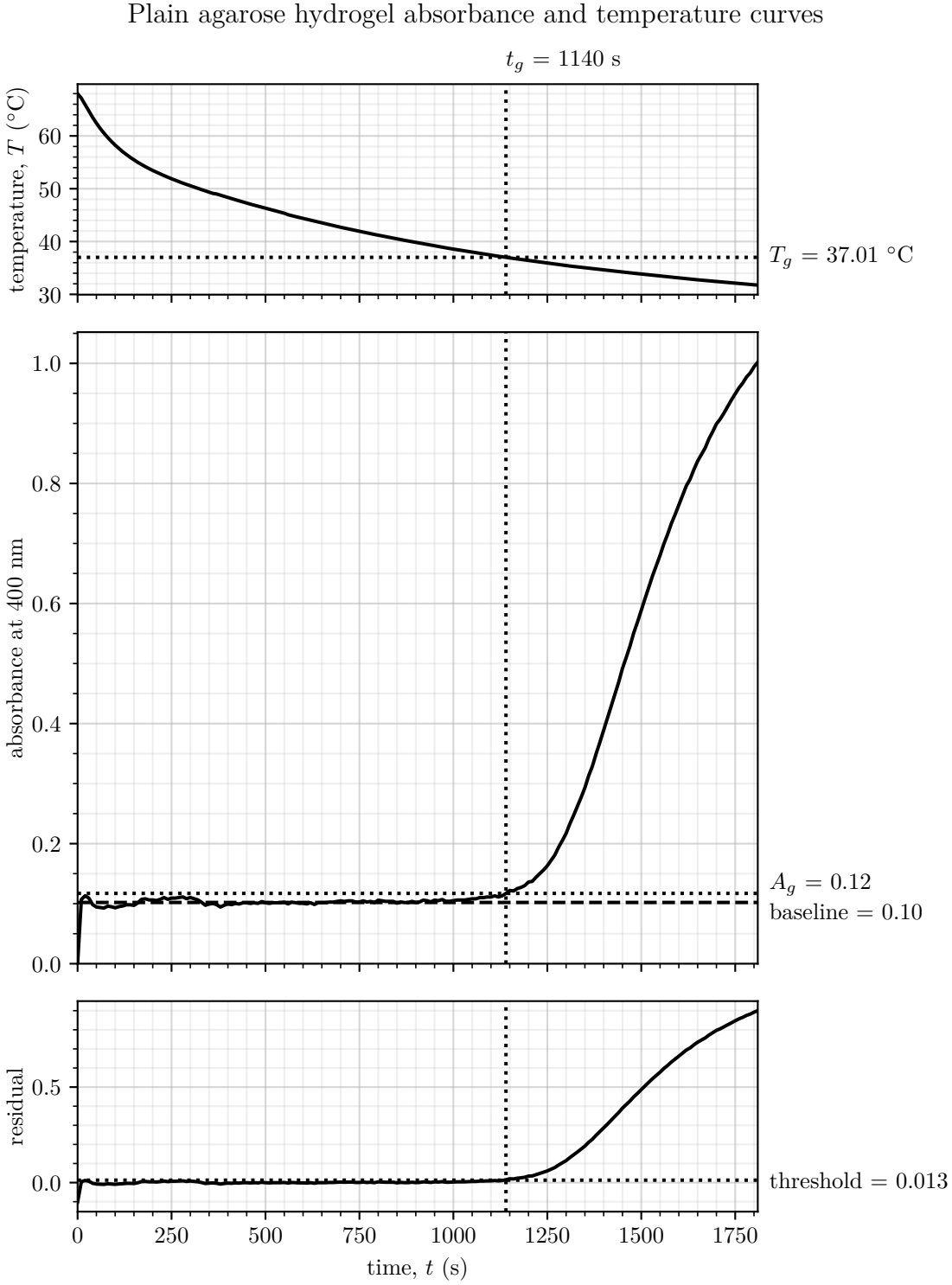

Figure 4: Plain agarose hydrogel absorbance and temperature curves

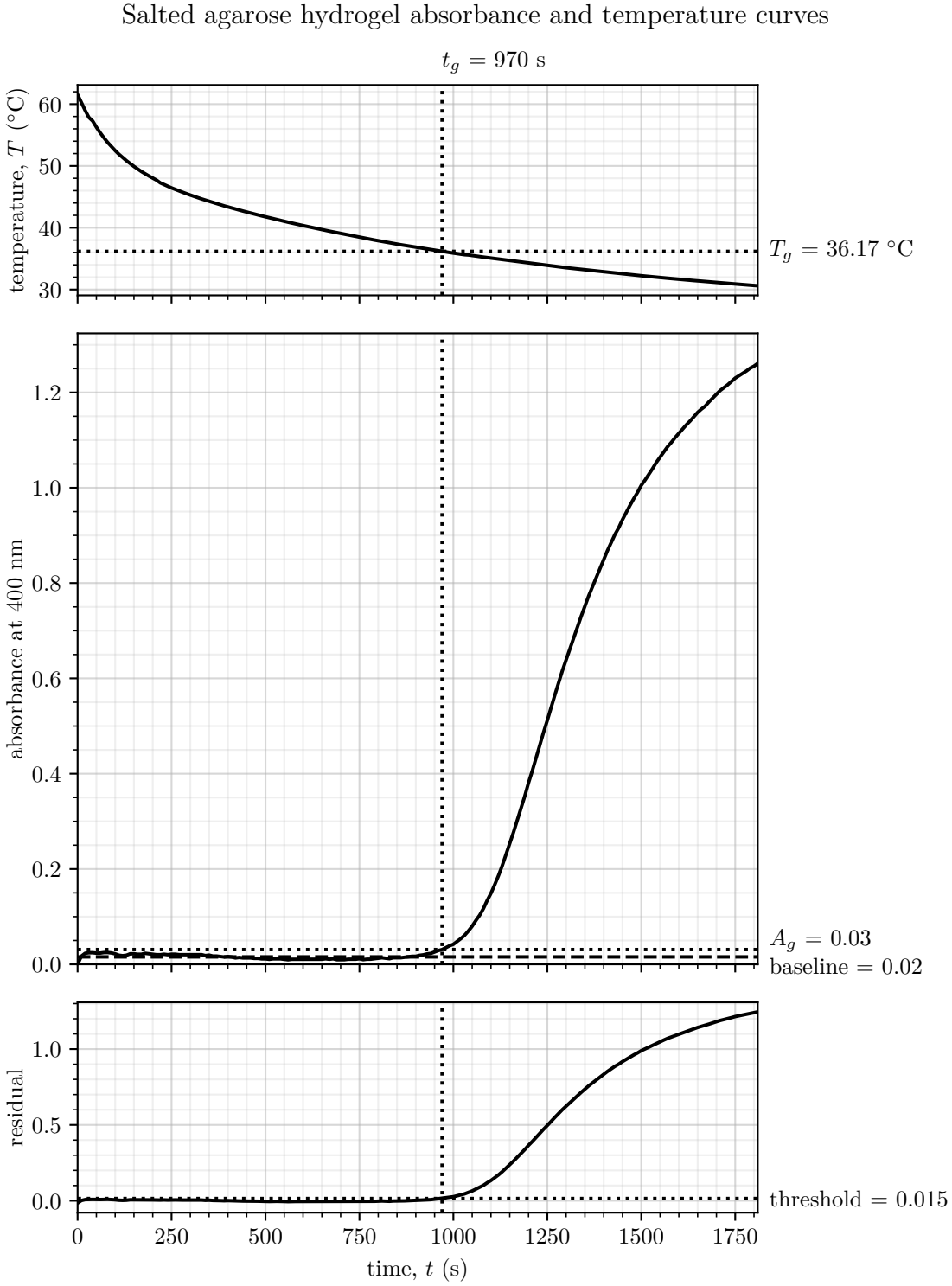

Figure 5: Salted agarose hydrogel absorbance and temperature curves

2.3 Mechanical measurements (S3)

2.3.1 Introduction

The deformation over time (i.e., creep) of plain and salted agarose hydrogels under two different loads (385 g and 925 g) was measured and model using the 4-component Burgers model. The compression setup was recorded using a mobile phone, and data was sampled from the recording after the experiment. The raw data is included in the appendix, under Table 4

The strain, ε, is defined as the change in length divided by the original length (i.e., $\frac{\Delta H}{H_0}$). H_0 of the agarose samples was 16 mm. σ_0 is calculated by dividing the force by the cross-sectional area of the agarose sample. The force was calculated from the mass of the weights using $F = mg$, where $g = 9.81\,\mathrm{m\,s^{-2}}$ is the acceleration due to gravity. The cross-sectional area of the agarose samples was calculated using $A = \pi r^2 = \pi \cdot 0.016^2 = 0.000201$ (3 s.f.). σ_0 for the two weights are summarised in Table 2. The creep compliance function was therefore computed for each time step as $\frac{\varepsilon}{\sigma_0}$, and the resulting calculations are outlined in Table 5.

mass, m (g)	force, F (N)	σ_0 (Pa)
385	9.065	18765
925	3.773	45086

Table 2: Values of σ_0 for the utilised loads

2.3.2 Plots and regression analyses

The $J(t)$ curves are plotted for each configuration in Figure 6, Figure 7, Figure 8, and Figure 9.

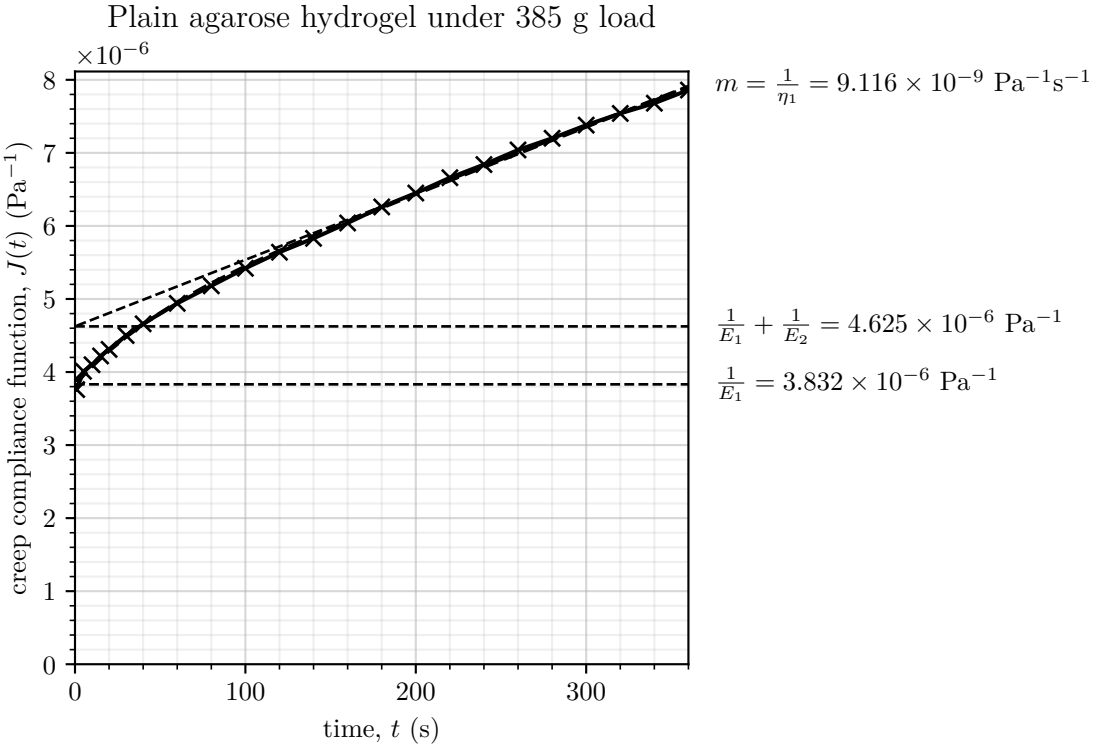

Figure 6: $J(t)$ against time for plain agarose hydrogel under 385 g load

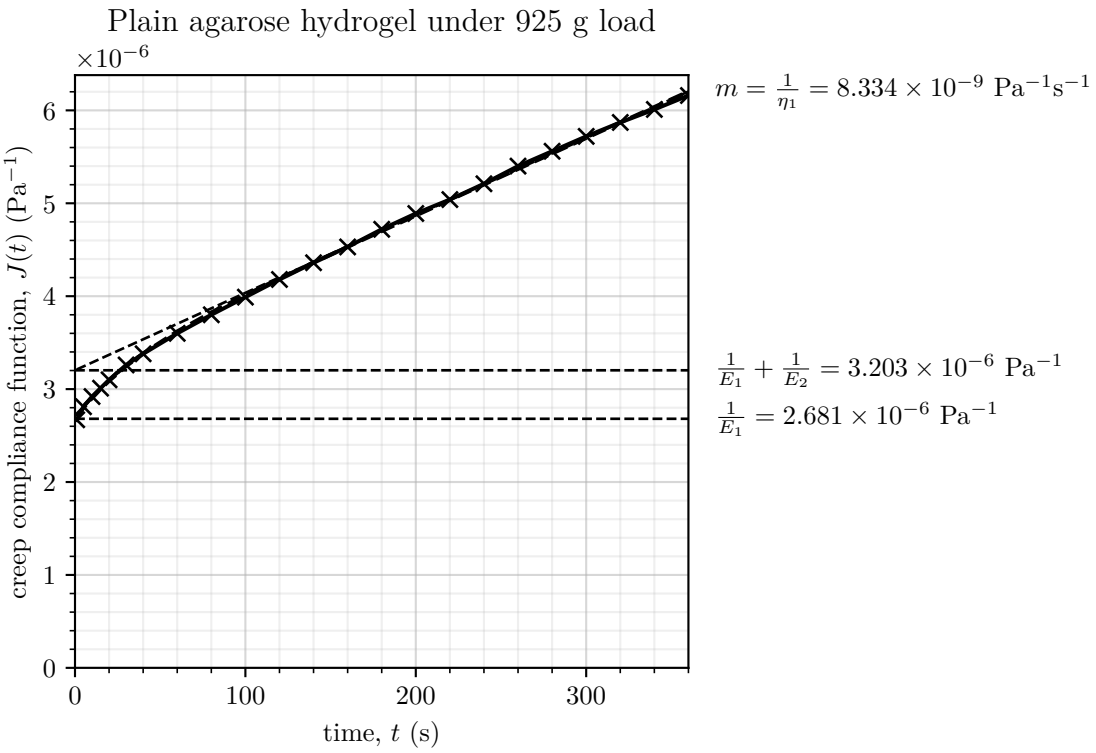

Figure 7: $J(t)$ against time for plain agarose hydrogel under 925 g load

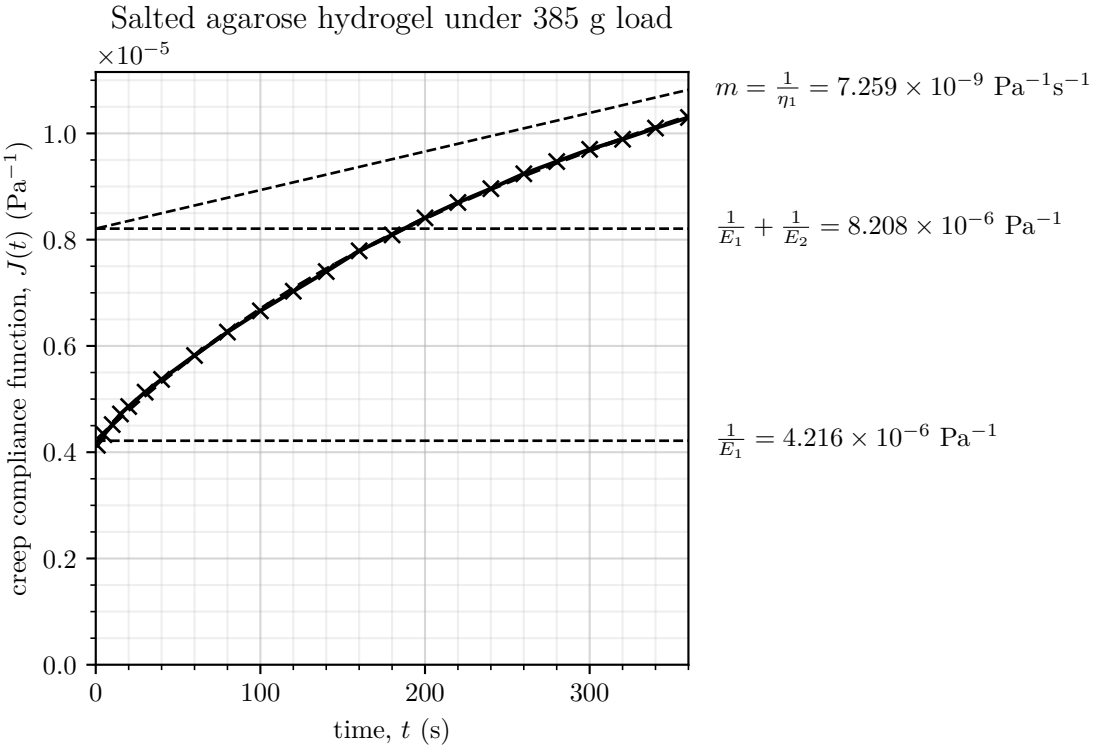

Figure 8: $J(t)$ against time for salted agarose hydrogel under 385 g load

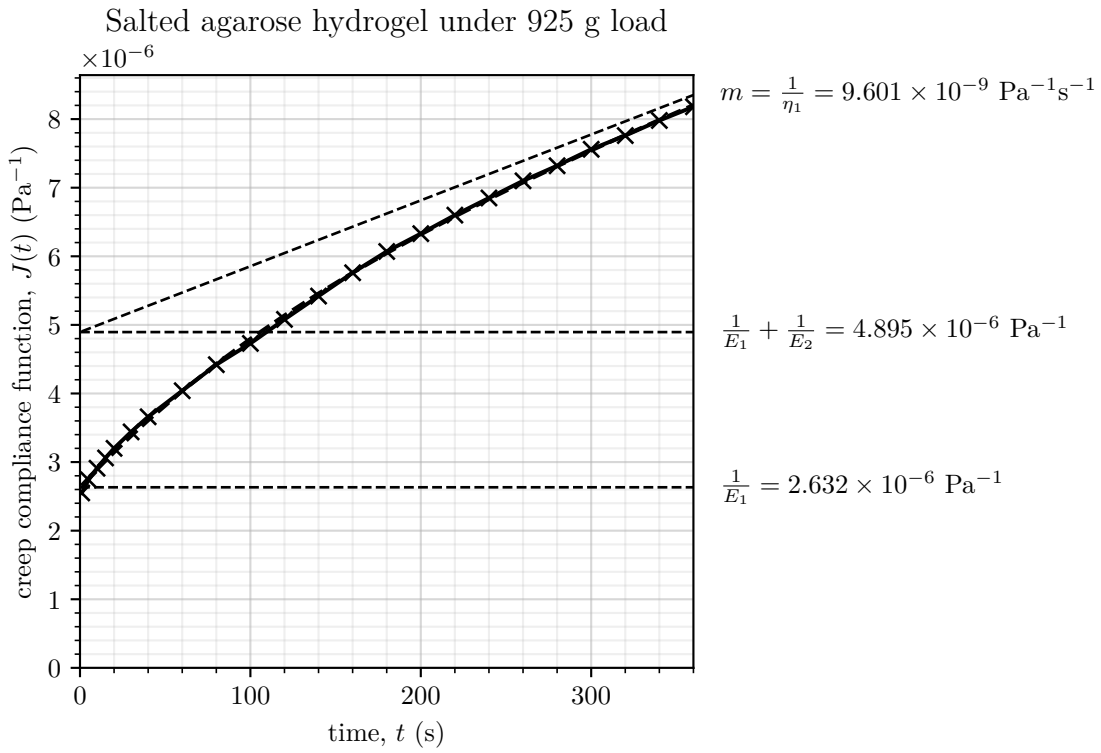

Figure 9: $J(t)$ against time for salted agarose hydrogel under 925 g load

For each set of calculated $J(t)$ values, we fit the model using `scipy.optimize.curve_fit` and the model definition stated in Figure 10.

$$J(t) = \frac{1}{E_1} + \frac{1}{E_2}\left[1 - \exp\left(-\frac{E_2 t}{\eta_2}\right)\right] + \frac{t}{\eta_1}$$

```
def maxwell_kevin_voigt_model(x, e_1, e_2, eta_1, eta_2):
    return 1 / e_1 + (1 / e_2) * (1 - np.exp(-e_2 * x / eta_2)) + x / eta_1
```

Figure 10: Definition and Python implementation of the Maxwell-Kevin-Voigt model of the creep compliance function

The fitted model is plotted as a dashed line. Horizontal lines are also plotted using the parameters yielded from the non-linear least squares regression. The linear region the model approaches for large t is plotted also as a line with equation:

$$y = \left(\frac{1}{\eta_1}\right)x + \left(\frac{1}{E_1} + \frac{1}{E_2}\right)$$

2.3.3 Results

The parameters of the model fits are outlined in Table 3.

	E_1 (kPa)	E_2 (MPa)	η_1 (GPa s)	η_2 (MPa s)
Plain, 385 g load	0.261	1.261	0.110	58.360
Plain, 925 g load	0.373	1.916	0.120	61.883
Salted, 385 g load	0.237	0.251	0.138	43.394
Salted, 925 g load	0.380	0.442	0.104	58.217

Table 3: Model parameters

The regression results are very close to the data points observed in Figure 6, Figure 7, Figure 8, and Figure 9; this demonstrates that the Burgers model is effective. The regression fits of all investigated configurations are plotted in Figure 11 for comparison.

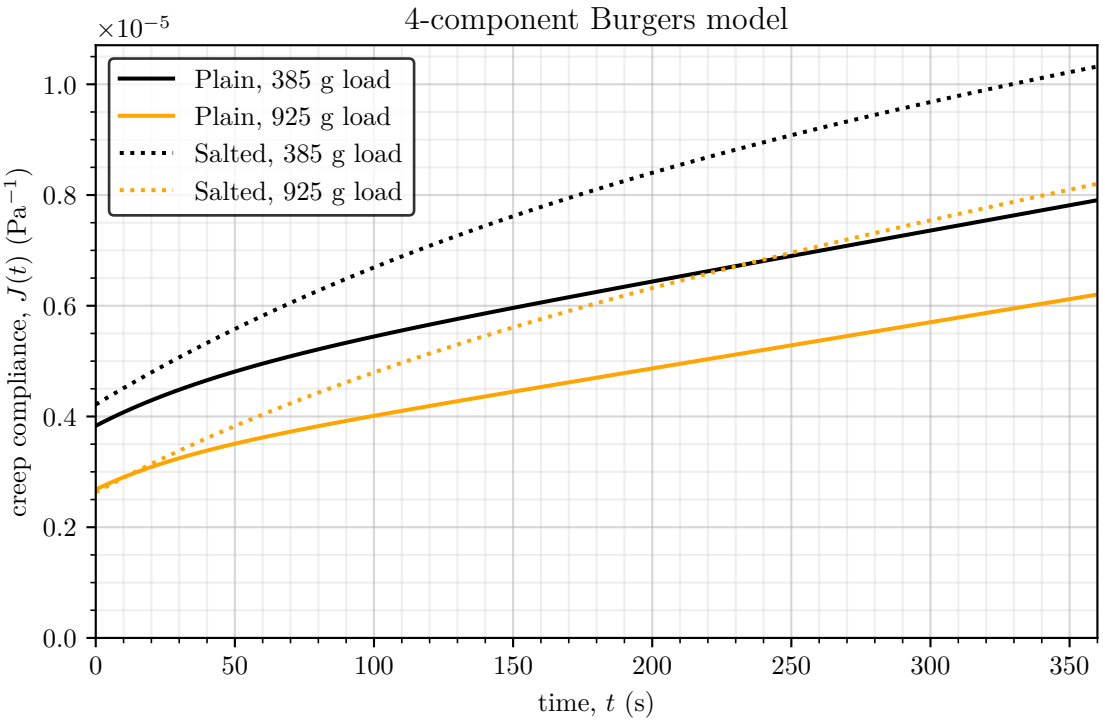

Figure 11: 4-component Burgers model fits overlaid on same axis

For a linear viscoelastic material, $J(t)$ is independent of stress, which means the material's response to any load can be effectively predicted by superposition. In the results, however, the parameters of the Burgers model change with the applied stress, and the higher load curves are not just scaled versions of the lower load curves. As a result, as $J(t)$ is observed to depend on stress, the material does not obey superposition and is therefore non-linear viscoelastic. It must be noted that the Burgers model fits and captures $J(t)$ well, even though linear superposition is invalid.

All configurations have relatively similar values for η_1, between 1 to 0.14. This suggests that the steady state, linear viscoous response is relatively invariant to σ_0 and salt content.

Other observations to note include:

- the salted samples generally have higher values for $J(t)$ than the plain agarose;
- for the same load, E_1 is very similar for both plain and salted agarose; however, E_2 varies greatly. E_1 is also greater for the higher load;
- for plain agarose, η_2 did not change very much with load, staying at approximately 60 MPa in comparison to the salted, which rose from 43 MPa to 58 MPa from the lighter to the heavier load; and
- visually, the samples were visibly deformed once the mass had been removed, with some edges buckling inwards, and the diameter enlarging in some areas.

2.3.4 Limitations

There are limitations of the method that may have introduced uncertainty into our observed creep compliance values. First, the agarose sample may not have been perfectly in line with the loading axis, which may have introduced an uneven stress profile across the cross-sectional area. In addition, there may be variations present in the initial height of the agarose samples. As a result, the metal spacer may not have been perfectly effective in either ensuring 0 initial stress (if the sample was taller than the spacer) or in preventing free fall of the mass pre-compression (if the sample was shorter than the spacer). Extraction of the metal spacer to initiate compression required supporting the mass from a point distant from the compression axis, allowing for a small initial tilt of the mass and an uneven initial application of load. Furthermore, there may be variation or human error in starting the stopwatch at the exact moment the load is applied.

2.4 Swelling measurements (S4)

2.4.1 Introduction

Swelling is investigated using a conventional gravimetric method on samples of plain agarose (3% w/v), salted agarose (1% $NaNO_3$), and gelatin (25% w/v). The samples are weighed and then immersed in water. At regular time intervals, they are taken out of the water, dried briefly with a consistent technique, and then weighed to capture the additional weight of water. The protocol is continued for an hour. Percentage swelling is calculated using the dry weight, W_d, and the sample weight, W_s:

$$\% \text{ swelling} = \frac{W_s - W_d}{W_d} \times 100$$

The percentage values for the three samples are included in the appendix, under Table 6.

2.4.2 The immersed hydrogel

Immersion of a hydrogel in a water allows for the hydrophillic groups common in natural hydrogels due to polypeptide structures (e.g., $-COOH$, $-NH_2$, $-OH$) to interact via hydrogen bonding with new water molecules as they diffuse into the network. The hydrogel swells and may increase in volume as the polymer expands to accommodate the entering water. A schematic of this process is outlined in Figure 12. In this schematic, note the condensed and relaxed conformation of the polymer chains (black lines), and the hydrogen bond interactions between water molecules and the hydrophillic groups.

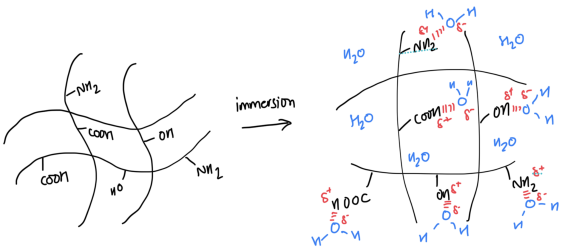

Figure 12: Schematic of the hydrogel immersion process

2.4.3 Results

The plots of the percentage of swelling against immersion time are displayed in Figure 13. The plain and salted agarose samples saturated with water quickly, demonstrated by the plateau at 1.75% on the graph for $t > 500$. Gelatin, however, did not saturate on the timescale the experiment was run (extended from 20min to 1 hour), and continued to increase swelling with immersion time. Therefore, the rate of change of mass of plain and salted agarose gels falls to 0 after 5 min, whereas gelatin's rate of change of mass appears to remain constant in this immersion time window.

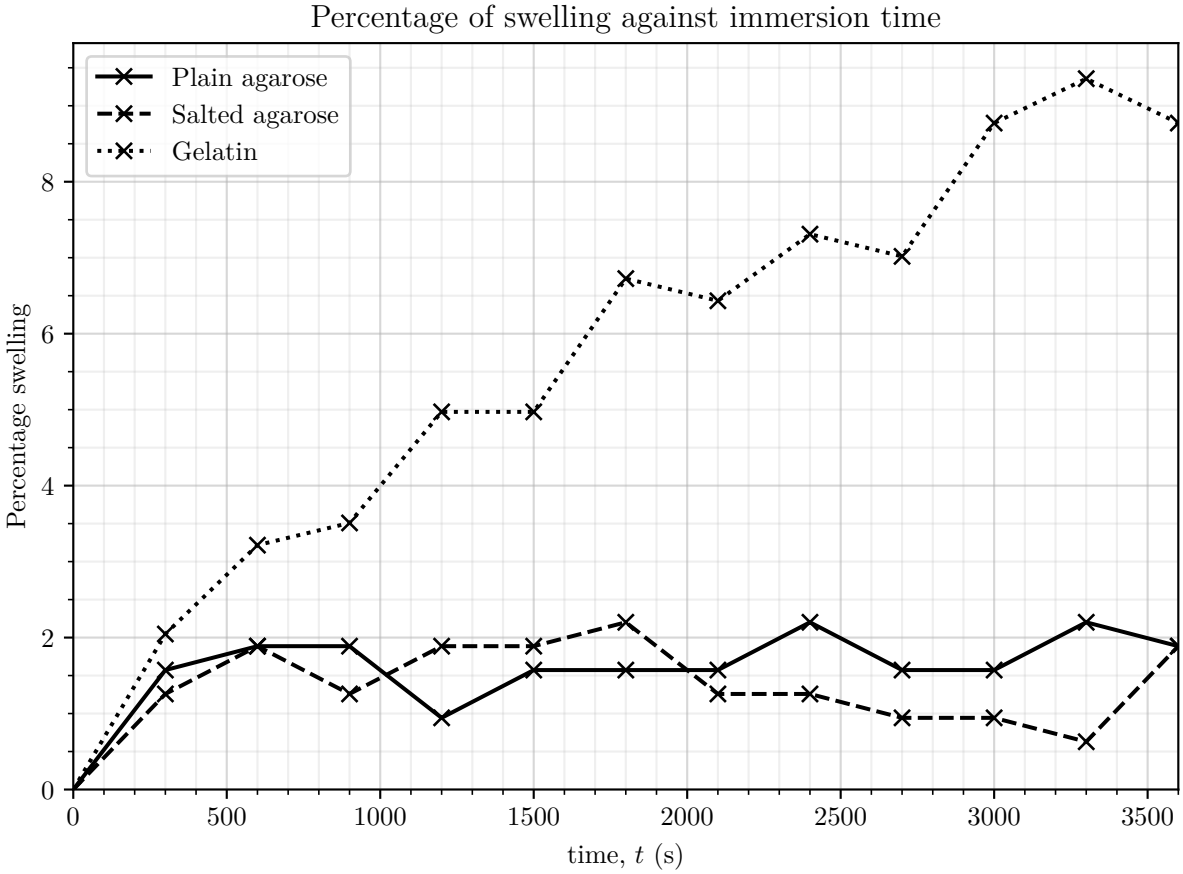

Figure 13: Percentage of swelling against immersion time for plain agarose, salted agarose, and gelatin

2.4.4 Limitations

Any variations in the technique used to dry the samples are likely to have introduced uncertainty in the measurements of W_s. Small amounts of human error may also have occurred in the timing of measurements, estimated to be on the order of 10 s. It was assumed that all samples were kept in comparable environmental conditions, such that their initial water content and subsequent approach to saturation were not differentially affected. Repeated mechanical handling with tweezers may have altered the internal structure of the gels or inconsistently displaced water through gentle squeezing. Finally, temperature was not actively controlled during the experiment, which may have influenced the rate of swelling.

2.5 Discussion

The literature quotes a gel point of 35 °C [4], and that the addition of salt does not modify the gelling point [5]. Two discrepancies arise, where we have found gelling points (stated in Table 1) with thermal methods approximately 20 °C greater than the literature values, and that we do see a difference between our plain and salted samples (2.1 °C in S1, and 0.8 °C in S2). [6] demonstrates that the coil-to-helix transition is sensitive to the percentage w/v of agarose, and literature figures state a range between 35 °C to 45 °C. Our values of 3% w/v agarose using optical methods finds values of T_g that are close to the literature values.

The differences between plain and salted agarose are within the margins of error of the thermocouple sensors and the limitations outlined in sections 2.1.3 and 2.2.3. The vastly different values of T_g we find could be a result of measuring different phenomena within the agarose. The coil-to-helix transition may occur over a period of time, a property that is not effectively captured in one temperature value in a data book; whether it is the temperature at which gelling begins, or ends, or somewhere inbetween is up for interpretation. The thermal method identifies the change in enthalpy response, which may occur earlier,

and the optical method used in S2 identifies changes in absorbance perhaps later in the transition process. As temperature continues to fall during the transition, this could lead to the discrepancies observed. Furthermore, as we produced the agarose ourselves by hand, uncertainties within the scales, measuring the volume of water, time in the microwave (and therefore intial temperature conditions) may affect our observations.

[7] provides evidence for non-linear viscoelastic behaviour, in line with our experimental observations. The non-linear viscoelastic behaviour may arise due to restructuring of the hydrogel in a stress-dependent manner via fibril bending, micro-buckling, or local network rearrangement. The literature corroborates the delayed elastic component with an explanation involving the bending of semiflexible fibrils; however, the non-linear behaviours described by the literature involving fibril stretching or slippage at fibril junctions were not observed in the range of stresses investigated. As a result, we don't see the deviations from the Burgers model. The increased values for $J(t)$ with the salted samples may be explained by the repulsive ionic interactions between salt ions and charged groups on the agarose chains loosening the the fibril network and increasing the pore size. The literature corroborates that increasing ionic strength increases mean pore size in agarose [8]. This relaxed network can provide less resistance to deformation, culminating in the observed greater fitted $J(t)$ for salted agarose.

The swelling trends remain in line with the literature. For agarose, we observed very little swelling, which aligns with swelling studies in [6], who also observed minimal swelling over the course of a much longer time period, 50 d. Gelatin, however, was observed to swell significantly, and did not decrease in rate in the hour long experiment. The literature also finds the swelling of gelatin to be a second order process [9]. The second order component, or the saturation of gelatin, may have only been observed with a longer experiment period. The ability for gelatin to swell with water is attributed to the gradient of water potential enabled by the soluble gelatin molecules within the insoluble network lowering water potential. In contrast, agarose does not feature this internal soluble protein content [10].

In general, these experiments featured no repeats, and therefore error bars could not be visualised or interpreted to understand the uncertainty and better differentiate two results as distinct or within the margin of error.

3 Conclusion

This study has provided insight into the characterisation of 3% w/v agarose hydrogels, both plain and salted with 1% $NaNO_3$. Thermal and optical measurements revealed the gelation transition, with differences between plain and salted samples falling within experimental uncertainty, highlighting the subtle effect of salt. Mechanical testing showed non-linear viscoelastic behaviour, with salted gels exhibiting slightly higher creep compliance, likely due to ionic interactions loosening the fibril network. Swelling experiments confirmed minimal water uptake in agarose compared to gelatin. Together, these results demonstrate how agarose network structure and ionic content govern gelation, mechanical response, and swelling, providing guidance for the design of agarose-based hydrogels in biomedical applications.

References

[1] Enas M. Ahmed. "Hydrogel: Preparation, Characterization, and Applications: A Review". In: *Journal of Advanced Research* 6.2 (Mar. 1, 2015), pp. 105–121. ISSN: 2090-1232. DOI: 10.1016/j.jare.2013.07.006. URL: https://www.sciencedirect.com/science/article/pii/S2090123213000969 (visited on 11/07/2025).

[2] Nuo Wang and Xue Shen Wu. "Preparation and Characterization of Agarose Hydrogel Nanoparticles for Protein and Peptide Drug Delivery". In: *Pharmaceutical Development and Technology* 2.2 (Jan. 1, 1997), pp. 135–142. ISSN: 1083-7450. DOI: 10.3109/10837459709022618. PMID: 9552439. URL: https://doi.org/10.3109/10837459709022618 (visited on 11/07/2025).

[3] Feng Jiang et al. "Extraction, Modification and Biomedical Application of Agarose Hydrogels: A Review". In: *Marine Drugs* 21.5 (May 2023), p. 299. ISSN: 1660-3397. DOI: 10.3390/md21050299. URL: https://www.mdpi.com/1660-3397/21/5/299 (visited on 11/07/2025).

[4] Valéry Normand et al. "New Insight into Agarose Gel Mechanical Properties". In: *Biomacromolecules* 1.4 (Dec. 1, 2000), pp. 730–738. ISSN: 1525-7797. DOI: 10.1021/bm005583j. URL: https://doi.org/10.1021/bm005583j (visited on 11/07/2025).

[5] Pasquale Sacco et al. "Ionic Strength Impacts the Physical Properties of Agarose Hydrogels". In: *Gels* 10.2 (Feb. 2024), p. 94. ISSN: 2310-2861. DOI: 10.3390/gels10020094. URL: https://www.mdpi.com/2310-2861/10/2/94 (visited on 11/07/2025).

[6] Marta Ghebremedhin, Sebastian Seiffert, and Thomas A. Vilgis. "Physics of Agarose Fluid Gels: Rheological Properties and Microstructure". In: *Current Research in Food Science* 4 (June 22, 2021), pp. 436–448. ISSN: 2665-9271. DOI: 10.1016/j.crfs.2021.06.003. PMID: 34258588. URL: https://pmc.ncbi.nlm.nih.gov/articles/PMC8255179/ (visited on 11/07/2025).

[7] Kia Bertula et al. "Strain-Stiffening of Agarose Gels". In: *ACS Macro Letters* 8.6 (June 18, 2019), pp. 670–675. DOI: 10.1021/acsmacrolett.9b00258. URL: https://doi.org/10.1021/acsmacrolett.9b00258 (visited on 11/07/2025).

[8] Nicolas Ioannidis et al. "Manufacturing of Agarose-Based Chromatographic Adsorbents – Effect of Ionic Strength and Cooling Conditions on Particle Structure and Mechanical Strength". In: *Journal of Colloid and Interface Science* 367.1 (Feb. 1, 2012), pp. 153–160. ISSN: 0021-9797. DOI: 10.1016/j.jcis.2011.10.063. URL: https://www.sciencedirect.com/science/article/pii/S0021979711013622 (visited on 11/07/2025).

[9] C. M. Ofner and H. Schott. "Swelling Studies of Gelatin. I: Gelatin without Additives". In: *Journal of Pharmaceutical Sciences* 75.8 (Aug. 1986), pp. 790–796. ISSN: 0022-3549. DOI: 10.1002/jps.2600750814. PMID: 3580032.

[10] John H. Northrop and M. Kunitz. "THE SWELLING PRESSURE OF GELATIN AND THE MECHANISM OF SWELLING IN WATER AND NEUTRAL SALT SOLUTIONS". In: *The Journal of General Physiology* 10.1 (Sept. 20, 1926), pp. 161–177. ISSN: 0022-1295. DOI: 10.1085/jgp.10.1.161. PMID: 19872305. URL: https://pmc.ncbi.nlm.nih.gov/articles/PMC2140869/ (visited on 11/07/2025).

Appendices

	displacement, ΔH (mm)			
time, t (s)	plain, 385 g	plain, 925 g	salted, 385 g	salted, 925 g
0	0.000	0.000	0.000	0.000
1	1.129	1.929	1.239	1.839
5	1.205	2.029	1.299	1.973
10	1.230	2.106	1.356	2.099
15	1.266	2.168	1.416	2.206
20	1.293	2.234	1.458	2.310
30	1.351	2.351	1.540	2.485
40	1.400	2.439	1.611	2.638
60	1.484	2.596	1.747	2.914
80	1.555	2.743	1.881	3.192
100	1.627	2.880	2.001	3.414
120	1.692	3.013	2.111	3.666
140	1.751	3.147	2.223	3.910
160	1.813	3.265	2.339	4.152
180	1.880	3.407	2.430	4.379
200	1.936	3.526	2.526	4.566
220	1.999	3.638	2.613	4.758
240	2.054	3.759	2.689	4.942
260	2.114	3.892	2.774	5.123
280	2.163	4.009	2.842	5.282
300	2.216	4.124	2.911	5.455
320	2.263	4.233	2.970	5.601
340	2.306	4.338	3.030	5.758
360	2.360	4.443	3.092	5.901

Table 4: S3 Raw observed displacement data for

	creep compliance function, $J(t)$ ($\times 10^{-6}$ Pa^{-1})			
time, t (s)	plain, 385 g	plain, 925 g	salted, 385 g	salted, 925 g
1	2.55	4.13	2.67	3.76
5	2.74	4.33	2.81	4.01
10	2.91	4.52	2.92	4.10
15	3.06	4.72	3.01	4.22
20	3.20	4.86	3.10	4.31
30	3.44	5.13	3.26	4.50
40	3.66	5.37	3.38	4.66
60	4.04	5.82	3.60	4.94
80	4.42	6.26	3.80	5.18
100	4.73	6.66	3.99	5.42
120	5.08	7.03	4.18	5.64
140	5.42	7.40	4.36	5.83
160	5.76	7.79	4.53	6.04
180	6.07	8.09	4.72	6.26
200	6.33	8.41	4.89	6.45
220	6.60	8.70	5.04	6.66
240	6.85	8.96	5.21	6.84
260	7.10	9.24	5.40	7.04
280	7.32	9.47	5.56	7.20
300	7.56	9.70	5.72	7.38
320	7.76	9.89	5.87	7.54
340	7.98	10.10	6.01	7.68
360	8.18	10.30	6.16	7.86

Table 5: S3 creep compliance values calculated from displacement data

time, t (s)	% swelling, plain	% swelling, salted	% swelling, gelatin
0	0.0	0.0	0.0
300	1.6	1.3	2.0
600	1.9	1.9	3.2
900	1.9	1.3	3.5
1200	0.9	1.9	5.0
1500	1.6	1.9	5.0
1800	1.6	2.2	6.7
2100	1.6	1.3	6.4
2400	2.2	1.3	7.3
2700	1.6	0.9	7.0
3000	1.6	0.9	8.8
3300	2.2	0.6	9.4
3600	1.9	1.9	8.8

Table 6: S4 percentage swelling of plain agarose, salted agarose, and gelatin over time